JOURNAL OF VIROLOGY, May 2010, p. 5270–5276 Vol. 84, No. 10
0022-538X/10/$12.00 doi:10.1128/JVI.00044-10

The Structure of Sindbis Virus Produced from Vertebrate and Invertebrate Hosts as Determined by Small-Angle Neutron Scattering▽

Lilin He,[1]† Amanda Piper,[2]† Flora Meilleur,[2,3] Dean A. A. Myles,[1,3] Raquel Hernandez,[2] Dennis T. Brown,[2] and William T. Heller[1]*

Center for Structural Molecular Biology and Chemical Sciences Division, Oak Ridge National Laboratory, Oak Ridge, Tennessee 37831[1]; Department of Molecular and Structural Biochemistry, North Carolina State University, Raleigh, North Carolina 27695[2]; and Neutron Scattering Sciences Division, Oak Ridge National Laboratory, Oak Ridge, Tennessee 37831[3]

Received 8 January 2010/Accepted 25 February 2010

The complex natural cycle of vectored viruses that transition between host species, such as between insects and mammals, makes understanding the full life cycle of the virus an incredibly complex problem. Sindbis virus, an arbovirus and prototypic alphavirus having an inner protein shell and an outer glycoprotein coat separated by a lipid membrane, is one example of a vectored virus that transitions between vertebrate and insect hosts. While evidence of host-specific differences in Sindbis virus has been observed, no work has been performed to characterize the impact of the host species on the structure of the virus. Here, we report the first study of the structural differences between Sindbis viruses grown in mammalian and insect cells, which were determined by small-angle neutron scattering (SANS), a nondestructive technique that did not decrease the infectivity of the Sindbis virus particles studied. The scattering data and modeling showed that, while the radial position of the lipid bilayer did not change significantly, it was possible to conclude that it did have significantly more cholesterol when the virus was grown in mammalian cells. Additionally, the outer protein coat was found to be more extended in the mammalian Sindbis virus. The SANS data also demonstrated that the RNA and nucleocapsid protein share a closer interaction in the mammalian-cell-grown virus than in the virus from insect cells.

Sindbis virus, a prototypic alphavirus, is an arbovirus that propagates between vertebrate hosts and invertebrate vectors during its natural cycle (1, 48). Sindbis virus consists of two nested icosahedral protein shells separated by a lipid membrane, all of which encapsulate a core containing single-stranded positive-sense RNA. The outer protein shell, composed of two glycoproteins, E1 and E2, associates with the interior nucleocapsid protein of the virus through specific interactions with the E2 endodomain (25–27, 36, 57, 62). Although the structure of Sindbis virus has been studied using electron cryomicroscopy (cryoEM) and X-ray scattering (12, 36, 49), providing important insight into its structure, differences in the structural features of Sindbis virus arising from the different virus host species have not been determined.

Certain structural features of the Sindbis virus are known to depend on the host species. Foremost among these differences are the glycosylation patterns that derive from the host (2, 20). The composition of the lipid membrane of the virus is also largely host determined (41, 42). Further, recent studies have demonstrated the importance of the host-derived membrane as a structural component of the virus particle (13, 15, 59). Similarly, viruses grown in insect cells have very little cholesterol compared to those grown in mammalian cells (11). *In vitro* studies with liposomes suggest that cholesterol plays an essential and critical role in the processes of entry and egress of viruses in living cells (28, 30, 39). The chimeric nature of Sindbis virus raises the possibility that other species-dependent differences in composition exist that drive additional host-specific differences in the structures of the viral components and in their assembly into the intact, functional virus. To determine if the virions from invertebrate or vertebrate host cells produce viruses with discernible structural differences, small-angle neutron-scattering (SANS) methods were applied to virus particles generated from mammalian baby hamster kidney (BHK) cells and mosquito C7-10 cells.

Small-angle scattering methods, which probe length scales ranging from 1 to 100 nm, are ideally suited to characterizing the structure of virus particles in solution (40, 51–53). While they do not provide structural information at atomic resolution, these techniques are very sensitive to the size and shape of biological macromolecules and complexes. SANS has additional benefits that stem from the interaction of neutrons with the samples (17, 50, 55, 61). The X-ray-scattering length of an atom, a measure of the interaction of an X-ray with an atom, depends on the atomic number, so small-angle X-ray scattering (SAXS) is dominated by the heavier elements present in a sample. In contrast, the neutron-scattering lengths of most elements are similar, making hydrogen simpler to visualize. Further, the scattering lengths of hydrogen and its isotope deuterium differ in sign, which makes it possible to dramati-

* Corresponding author. Mailing address: Center for Structural Molecular Biology and Chemical Sciences Division, Oak Ridge National Laboratory, P.O. Box 2008, MS-6393, Oak Ridge, TN 37831. Phone: (865) 241-0093. Fax: (865) 574-6268. E-mail: hellerwt@ornl.gov.
† L.H. and A.P. contributed equally to this work.
▽ Published ahead of print on 10 March 2010.

cally change the scattering-length density of a biological macromolecule or an aqueous buffer by substituting deuterium for hydrogen. The scattering-length densities of proteins, lipids, and nucleic acids differ naturally, making it possible to probe the internal structures of virus particles with SANS (3, 5–8, 16, 18, 21–23, 44). Another important feature of SANS is that neutrons produce far less radiation damage in biological materials than X rays, making it possible to study delicate systems without fear of impacting the results. Samples studied by SANS can be further characterized for structure and function, such as viral infectivity, after the completion of the SANS measurements.

In the present work, SANS was used to investigate differences in the structure of Sindbis virus that resulted from two host cell species. Virus particles grown in mammalian (BHK) and insect (*Aedes albopictus* clone C7-10) cells were compared to determine if host-derived structural differences exist alongside the known host-specific compositional differences (11). To maximize the scattering power of the virus, measurements were performed on BHK and C7-10 Sindbis virus particles purified in 100% D_2O. The SANS data demonstrate that the BHK virus particle is larger than the C7-10 insect cell particle. The radial-scattering-length density profile determined from the SANS data demonstrates that while the BHK virus particle's lipid layer contains considerably more cholesterol than that of the C7-10 virus, the radial position of the lipid layer does not differ significantly between the two host species. Further, the nucleocapsid core of the particle, which contains protein and nucleic acid, shows structural differences between the two host species. The SANS data also indicate that the outer coat protein is more extended in the BHK-derived virus particle than in the C7-10-derived virion. These results are the first demonstration of structural differences in Sindbis viruses arising from different virus host species and suggest that a structural basis exists for the observed differences in the particles. The biological implications of these differences are unknown, because no differences in infectivity were seen between BHK and C7-10 cell-derived Sindbis viruses.

MATERIALS AND METHODS

Growth of virus. Virus was grown in BHK cells as previously described (14). Forty 75-cm^2 flasks were infected at a multiplicity of infection of 10 PFU/cell and were completed with 6 ml of medium, which was harvested 24 h postinfection. The 240 ml of harvested supernatant was subsequently purified via isopycnic ultracentrifugation on potassium tartrate gradients (11). Virus was also prepared similarly in C7-10 mosquito cells, with the exception that the supernatant of mosquito cells was harvested 48 h postinfection rather than 24 h.

Ultracentrifugation and virus purification. Virus was purified using three subsequent ultracentrifugation gradients. First, 20 ml of supernatant was loaded on top of a step gradient comprised of a 15% potassium tartrate step solution in phosphate-buffered saline (PBS) made in D_2O (PBS-D) (1.47 mM KH_2PO_4, 0.14 M NaCl, 80 mM $Na_2HPO_4 \cdot 0.7H_2O$ at a potentiometric deuterium ion concentration [pD] of 7.2) over a 37% potassium tartrate solution in PBS-D. After centrifugation in an SW28 Beckman rotor at 24,000 rpm for a minimum of 14 h, virus bands were pulled from the gradients and diluted at a ratio of 1:2 with PBS-D. The diluted virus bands were then loaded into a linear potassium tartrate gradient ranging from 15% potassium tartrate in PBS-D to 37% potassium tartrate in PBS-D. These linear gradients were centrifuged for a minimum of 4 h at 24,000 rpm. The virus bands were pulled from the second gradient. After the virus was purified using the second gradient, all subsequent solutions used were made using D_2O instead of H_2O. The virus was diluted 1:2 once again with PBS-D and loaded onto a third and final step gradient. The third gradient contained a 12% to 33% step gradient of potassium tartrate in PBS-D and D_2O. Virus removed from this gradient should not have contained water, which is less dense than D_2O. Therefore, the virus was considered suitable for analysis by neutron scattering. A refractometer was used to measure the refractive index of the purified virus. The same 12% and 33% potassium tartrate solutions used in the third purification gradient were then mixed to generate a blank (virus-free) solution that possessed the same refractive index as the purified virus. This solution had a final potassium tartrate concentration of 22%. Prior to delivery of the purified virus to Oak Ridge National Laboratory, the protein concentration, titer, and particle/PFU ratios of the virus were determined. Negative stains of virus were also observed using scanning electron microscopy to ensure that the particles were intact. Virus titers were also determined after the virus had been in the beam for each of the samples measured. The particle-to-PFU ratio (a measurement of infectivity) was determined to be near unity, ensuring that the virus studied was infectious.

SANS measurements. The SANS experiments were performed using the BioSANS (CG3) of the high-flux isotope reactor of the Oak Ridge National Laboratory (29). Samples were measured at room temperature in sealed, 1-mm-path-length quartz cuvettes at concentrations of ~500 μg/ml for BHK and ~400 μg/ml for C7-10 samples. The neutron wavelength was set to 6 Å with a wavelength spread, $\Delta\lambda/\lambda$, of 0.14. Scattered neutrons were detected with a 1- by 1-m helium-filled two-dimensional (2D) position-sensitive detector with 192 by 192 pixels. Two sample-to-detector distances, 6.8 m and 15.2 m, were used to cover a q range between q_{min}, 0.003 $Å^{-1}$, and q_{max}, 0.16 $Å^{-1}$, where q is the magnitude of the scattering vector and is equal to $4\pi \sin(\theta)/\lambda$ and 2θ is the scattering angle. The samples and corresponding buffers were collected for approximately 3 h at each detector setting to obtain acceptable counting statistics. The raw 2D data were corrected for the detector pixel response and dark current, which represent the ambient radiation background and electronic noise, before being azimuthally averaged to produce the 1D scattered-intensity profile, $I(q)$ versus q. The data were placed on an absolute scale (cm^{-1}) through the use of calibrated standards (60). The reduced 1D profiles from the two detector distances were merged using software developed by the National Institute of Standards and Technology (NIST) (19) implemented in Igor Pro 6.1 (WaveMetrics, Lake Oswego, OR). The reduced and merged data were produced by subtracting the $I(q)$ for the buffer from that of the sample and including a constant to account for the difference in incoherent scattering that arises from the difference in hydrogen content that results from the displacement of buffer by the virus in the sample.

SANS data analysis. The data were analyzed according to the method of Guinier for the radius of gyration, R_g (10). R_g is a model-independent parameter that provides a measure of the compactness of a particle. Guinier analysis utilizes a series expansion of $I(q)$ to derive an approximate Gaussian form for the intensity.

$$I(q) \propto I(0)\exp(-q^2R_g^2/3) \quad (1)$$

A linear fit of $\ln(I(q))$ versus q^2 provides the intercept and slope, which are related to the zero-angle scattering intensity, $I(0)$, and R_g, respectively. The expansion used to derive the Guinier approximation is applicable to only a limited range of low q values. For a nearly spherical particle, such as that of Sindbis virus, the approximation is valid for a value of $q \cdot R_g$ of <1.3 (53).

The second model-independent analysis applied to the SANS data was to determine the excess radial-scattering-length distribution function. For a spherically symmetric particle, the scattering-length density relative to that of the solvent, $\rho(r) - \rho_s$, can be determined by performing a Fourier transform of the structure factor, $F(q)$, through equation 2.

$$\rho(r) - \rho_s = \frac{1}{2\pi r}\int_0^\infty q \cdot F(q) \cdot \sin(qr) \cdot dq \quad (2)$$

$F(q)$ is related to the scattering intensity by the equation $I(q) = |F(q)|^2$. While the intensity is strictly a positive number, it is possible for $F(q)$ to be either positive or negative. $F(q)$ is a continuous function, and therefore, the sign alternates from positive to negative smoothly. It was assigned to alternate after each sharp minimum in the measured profile. Previous researchers found that $\rho(r) - \rho_s$ is not reliable at short distances due to truncation errors that result from performing a Fourier transform over a limited q range and deviations from true spherical symmetry (4, 18). Here, the entire measured q range was used for the Fourier transform. The direct transformation of the data into $\rho(r) - \rho_s$ prevented taking the instrument resolution into account.

Data were also fitted for the distance distribution function, $P(r)$, which is the frequency of all pairwise distances within a scattering particle, weighted by the

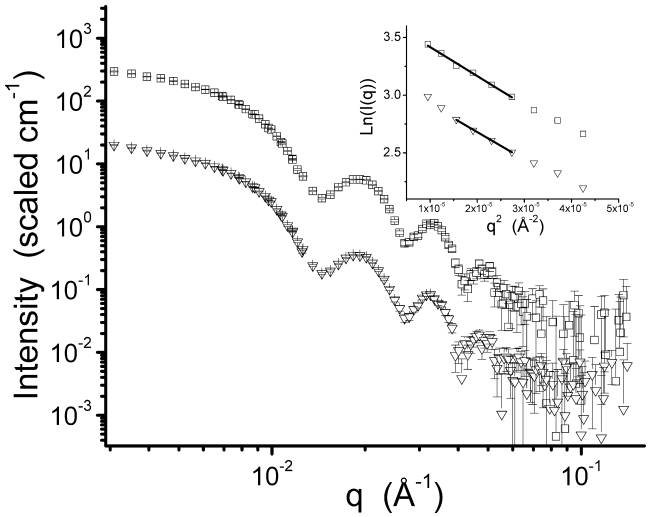

FIG. 1. SANS patterns of BHK (□)- and C7-10 (▽)-grown Sindbis particles in potassium tartrate buffer at pD 7.2. The Guinier plots for BHK (□) and C7-10 (▽) are shown in the inset. Superimposed are best-fit straight lines, determined by the least-squares procedure, which were used to estimate the radius of gyration, R_g, and zero-angle scattering intensity $I(0)$. The data have been offset for clarity.

scattering-length density difference relative to the solvent. $P(r)$ is related to $I(q)$ through equation 3.

$$P(r) = \frac{1}{2\pi^2}\int_0^\infty qr \cdot I(q) \cdot \sin(qr) \cdot dq \quad (3)$$

$P(r)$ was evaluated using the indirect Fourier transform method implemented in the program GNOM (45). The instrument resolution effects that result from the sizes of the apertures and their separation, as well as the wavelength spread used, were taken into account in the fitting, making it possible to fit the data collected at both detector distances simultaneously. The fitting of the maximum linear dimension of the scattering particle, D_{max}, and the second moment of $P(r)$ is the square of the R_g of the particle.

A multishell spherical model was also applied to the data to better understand the radial distribution of material in the virus. While Sindbis virus is known to be an icosahedral particle, EM studies suggest that the particle has a strongly spherical character, making it reasonable to model the structure of the virus with concentric spherical shells (12, 36, 62). The intensity profile of the multishell model is given by equation 4.

$$I(q) = \frac{\phi}{V_p}\left[\sum_{i=1}^{N}\frac{3V_i(\rho_i - \rho_{i+1})j_1(qr_i)}{qr_i}\right]^2 + bkg \quad (4)$$

The volume fraction of the particles in solution is ϕ, V_p is the volume of the virus particle, and V_i and R_i are the volume and radius of the ith concentric sphere, respectively. N is the number of shells used. The spherical Bessel function is given by $j_1(x) = (\sin x - x \cos x)/x^2$. The retuned value is scaled to units of cm^{-1}, and the additive background is applied. The free parameters for the model fitting were the radii of the shells and the scattering-length density of each shell. Fitting was accomplished through the use of a modified version of the nonlinear least-squares fitting routines developed by NIST (19) in the IgorPro software package. The instrument resolution function was accounted for in the modeling. The initial values for the scattering-length density and thickness of each shell were estimated from the previously published cryoEM structure of Sindbis virus (12, 36, 62). In order to determine the ideal number of shells for the fitting, different values of N were tested. It was determined that a minimum of four shells are required to adequately fit the data. Using more than four shells did not significantly improve the quality of the fit to the data. Therefore, the results for the multishell fitting with four shells are presented here.

RESULTS AND DISCUSSION

The SANS profiles of BHK and C7-10 particles in potassium tartrate buffer in 100% D_2O at pD 7.2 are shown in absolute units in Fig. 1. The profiles have the central maximum at a q of 0, followed by three clearly distinguishable subsidiary maxima that are typical of scattering from a predominantly spherical particle. The higher-order peaks are lost in the noise as a result of the limitations of the incident flux, the available beam time, and the broader instrument resolution function at the shorter instrument configuration that provides the data at higher q values. The differences between the scattering from the BHK and C7-10 virus particles are subtle and can be seen below 0.05 Å^{-1}. The differences in the $I(0)$ values resulted primarily from the differences in the sample concentrations, with any possible differences in composition of BHK and C7-10 viruses being a secondary effect. Analysis of the samples after exposure to the neutron beam determined that there was little to no loss of infectivity during the time that the samples were in the beam—4×10^{13} PFU/ml for the BHK virus before and after exposure—while the C7-10 samples were 1×10^{14} PFU/ml before and after the SANS experiment. In addition, we also determined that there was no loss of viral material through interactions with the cuvettes. Therefore, we are confident that the structural differences observed were not induced by radiation damage.

The results of the Guinier fitting of the SANS data for the BHK and C7-10 virus particles for R_g are shown in the inset in Fig. 1, and the R_g and $I(0)$ values are summarized in Table 1. Although the number of data points in the Guinier region is limited due to the size of the Sindbis virion, the data quality at low q provides small uncertainties, in a relative sense, in the extracted parameters. The Guinier plot of the BHK data exhibits good linearity, suggesting that the solution was reasonably free from larger aggregates or very high-molecular-weight contaminants. The C7-10 sample shows very minor indications of high-molecular-weight contaminants or aggregates of the virus; therefore, the first two data points were excluded from the fitting reported in Table 1. The minor deviations from a truly monodisperse sample actually cause the R_g for the C7-10 virus to appear slightly larger than it actually is, but the truncation of the low-q portion of the range used for the fitting minimizes this effect. The Guinier fitting performed did not take the instrument resolution function into account, but the difference in R_g was not impacted by it. The R_g values extracted from the data indicate that the BHK virus was less compact than the C7-10 virus. In light of the general similarity of the structures based on the scattering data, which were approximately spherical, and the very similar material compositions of the two virions, it is possible to conclude from the Guinier fitting that the material in the BHK virus was less localized at the center of the particle, on average.

TABLE 1. R_g and $I(0)$ values of the BHK- and C7-10-grown Sindbis particles from a Guinier approximation

Sample	R_g (Å)	$I(0)$ (cm^{-1})
BHK	277.0 ± 8.0	39.44 ± 0.97
C7-10	267.5 ± 3.0	23.50 ± 0.27

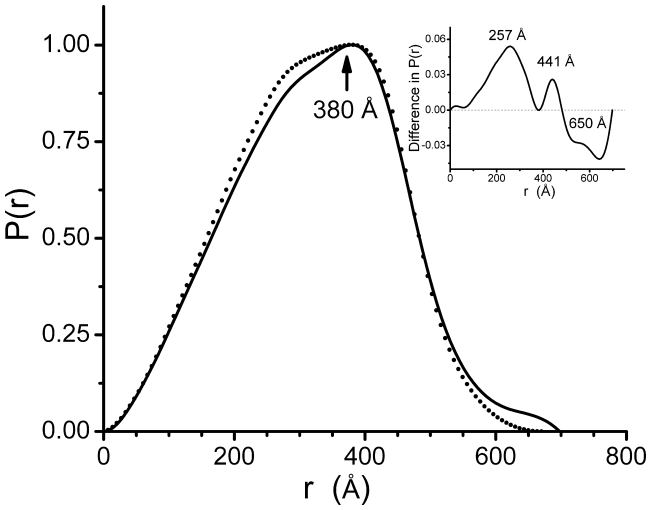

FIG. 2. Distance distribution functions, $P(r)$, of BHK (solid line)- and C7-10 (dotted line)-grown Sindbis particles. The inset plot shows the difference in $P(r)$ values of two particles.

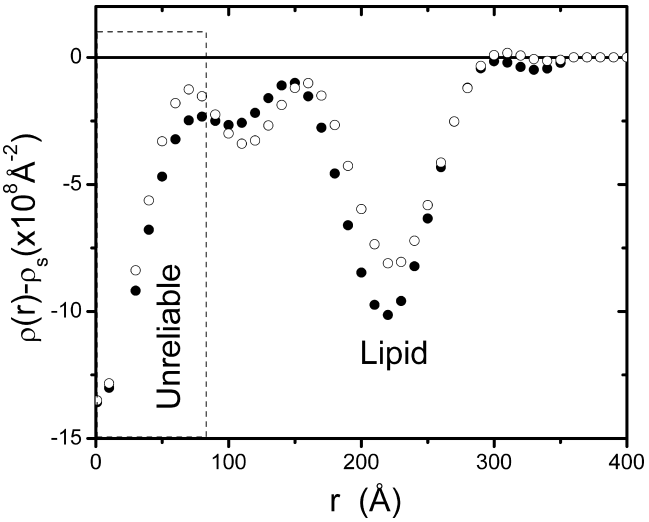

FIG. 3. Radial-scattering-length-density distribution function of BHK (●)- and C7-10 (○)-grown Sindbis particles.

To gain further insight into the nature of the difference between the BHK and C7-10 particles, the data were fitted for $P(r)$ using the program GNOM (45), the results of which are shown in Fig. 2. The $P(r)$ curves were normalized to a peak height of 1.0 to provide an easier comparison. The R_g, $P(r)$, and D_{max} values determined by the fitting are presented in Table 2. Again, the R_gs of the two particles indicate that the BHK virion is less compact than the C7-10 virion. The discrepancy between these values and the R_gs determined by Guinier analysis can be attributed to the instrumental-resolution function and the use of the entire range of data for determining $P(r)$. Both $P(r)$ curves have a single broad, asymmetric peak centered near 350 Å. The $P(r)$ of the BHK particle exhibits a more pronounced asymmetric shape clearly suggestive of a superposition of two broad peaks, while the C7-10 $P(r)$ has a better-defined, single maximum. The shift in the peak to larger distances for the BHK particle supports the idea that the mass in the particle was less centralized than it was in the C7-10. The $P(r)$ fitting demonstrates that the BHK particle (D_{max} = 698 Å) had a larger diameter than the C7-10 particle (D_{max} = 670 Å). The uncertainty in the D_{max} determined using GNOM was estimated to be ~5% for these data sets. The difference between the two $P(r)$ curves, specifically the C7-10 curve minus the BHK curve, is shown in the inset plot in Fig. 2 and shows a clear difference in the distribution of mass. The C7-10 particle shows additional material at shorter distances and less material at the longer vector lengths in the particle. The nature of the $P(r)$ prevents a clear discussion of exactly how the structure of the virus differs based solely on this analysis.

The radial-scattering-length density distribution functions, $\rho(r) - \rho_s$, which are shown in Fig. 3, were determined in order to better understand the internal structure of the particles. The curves below ~90 Å were considered unreliable due to the nature of the fitting (4, 18). Both curves have a single prominent feature, the broad minimum between 200 Å and 250 Å. The single minimum is dominated by the lipid in the virus, which has a lower scattering-length density than the RNA or the protein, as can be seen in Table 3. The positions differ slightly, being ~215 Å in the BHK virus and ~225 Å in the C7-10 virus, both of which are consistent with the cryoEM structure of Sindbis virus (12, 62). The difference in the depths of the minima is indicative of a difference in composition. Of the Sindbis virus components listed in Table 3, only cholesterol is capable of lowering the scattering-length density of the lipid layer. This reduction in the scattering-length density increases the contrast of the lipid layer relative to the solvent. The $P(r)$ values determined are weighted by the contrast of the materials present in the scattering particle. Therefore, some of the difference between the R_gs of BHK and C7-10 can be attributed to the increased scattering contrast resulting from the differences in the cholesterol contents of the lipid layers. The results are consistent with recent work demonstrating that the BHK virus contains considerably more cholesterol than the C7-10 virus (11). The other features in the curves suggest a redistribution of material, but the effect is subtle in this fitting

TABLE 2. R_g, $I(0)$, and D_{max} values of the BHK- and C7-10-grown Sindbis particles from GNOM (45)

Sample	R_g (Å)	$I(0)$ (cm^{-1})	D_{max} (Å)
BHK	246.6 ± 0.7	35.67 ± 0.21	698
C7-10	240.6 ± 0.8	23.35 ± 0.16	670

TABLE 3. Scattering-length densities of components of Sindbis virus in 100% deuterated solvent[a]

Component	SLD[b] (10^{-6} Å^{-2})
RNA	4.41
Capsid protein	3.17
Lipid	0.59
Cholesterol	0.17
Glycoprotein	3.00
Solvent	5.23

[a] Actual percentage was 95.7% due to the protonated potassium tartrate that was used.
[b] SLD, scattering-length density.

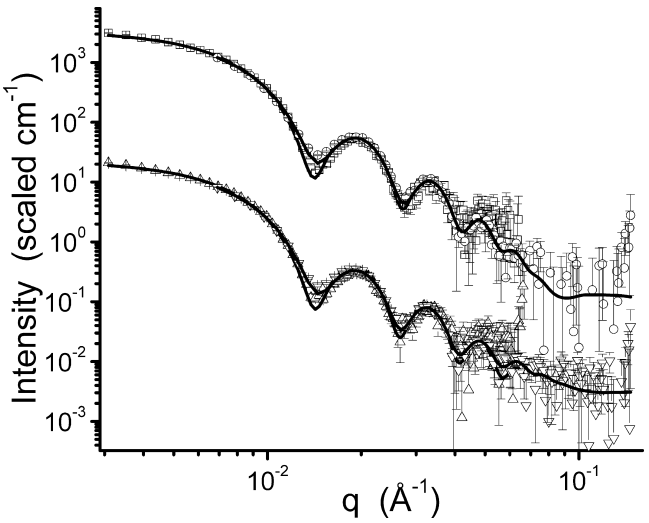

FIG. 4. Four-shell model for BHK (□, low-q data; ○, high-q data)- and C7-10 (△, low-q data; ▽, high-q data)-grown Sindbis particles in potassium tartrate at pD 7.2. The solid line in each curve corresponds to the best fit using the multishell model. The curves have been offset for clarity, further than in Fig. 1.

and is complicated by the unreliability of the curves at the smaller radii.

To obtain a better picture of the distribution of material within the two virus particles, the data were fitted using a 4-shell spherical model in which the scattering-length densities and the radii of the shells were allowed to freely vary. The model profiles are shown with the SANS data from the BHK and C7-10 viruses in Fig. 4. The impact of the resolution function on the model curves (the lines overlaid onto the data) can be clearly seen, particularly at the first minimum in the data sets. The radii and scattering-length densities determined by the model fitting for BHK and C7-10 viruses are summarized in Tables 4 and 5, respectively, along with the material content interpreted from the results. The larger uncertainties, in both an absolute and a relative sense, of the structural parameters determined for the inner shells result from their relative volumes in the structure. We estimate an ~20-Å uncertainty in the total particle radius that is strongly coupled to the uncertainties in the various shell radii of the model. The model fitting found a radius of 340 Å (680-Å diameter) for the BHK virus, which is consistent with the value in the literature (12, 36), while the C7-10 virus was smaller, with a 320-Å radius (640-Å diameter). Both results are in agreement with other analyses presented here.

TABLE 4. Fitting parameters from a four-shell model for BHK-grown Sindbis particles and possible components in each shell[a]

Shell no.	Thickness (Å)	SLD (10^{-6}Å^{-2})	Components
1	90.87 ± 10.81	4.02 ± 0.15	RNA, solvent
2	100.41 ± 12.10	4.65 ± 0.09	Solvent, some RNA, capsid protein
3	69.64 ± 2.02	1.49 ± 0.08	Lipid, protein, cholesterol
4	79.28 ± 1.59	4.74 ± 0.06	Extended glycoprotein, solvent

[a] Total radius, 340.20 ± 16.40 Å.

TABLE 5. Fitting parameters from a four-shell model for C7-10-grown Sindbis particles and possible components in each shell[a]

Shell no.	Thickness (Å)	SLD (10^{-6}Å^{-2})	Components
1	130.02 ± 12.61	4.03 ± 0.08	RNA, solvent
2	57.16 ± 13.01	5.10 ± 0.82	Solvent, some capsid protein
3	71.43 ± 3.10	2.22 ± 0.30	Lipid, protein
4	61.76 ± 2.01	4.52 ± 0.14	Glycoprotein, solvent

[a] Total radius, 320.37 ± 18.49 Å.

The shells, loosely ascribable to the RNA core, inner capsid, lipid bilayer, and outer capsid, have thicknesses that are in reasonable agreement with the cryoEM structure (62). The results demonstrate that there are differences in the distribution of material that depend on the cell species. In both particles, an ~70-Å-wide layer starting at ~190 Å had a significantly lower scattering-length density than the other layers, making it possible to assign it to the lipid layer of Sindbis virus. The difference in the density of this layer again demonstrates that the cholesterol incorporated into Sindbis virus by the host species (11) associates with the lipid layer. A typical phospholipid bilayer has a thickness of roughly 50 Å (34), suggesting that this layer does not consist solely of lipids and cholesterol. The increased thickness of the layer is likely the result of protein organization near the surface of the lipid layer, which is reasonable in light of the known association of the nucleocapsid protein with the E1 and E2 proteins from the outer capsid (25–27, 36, 57, 62). The outermost shell, which is dominated by the outer envelope glycoproteins of Sindbis virus, is more extended in the BHK virus than in the C7-10 virus, as evidenced by the larger radius and higher average scattering-length density that would result from solvent penetration into this layer. One possibility is that the BHK outer-envelope proteins are in a more extended conformation than those in the C7-10 virion. The virus glycoproteins are glycosylated by host cell enzymes, suggesting that alterations in the pattern of glycosylation may account for the differences in virus structure. Insect cells lack the enzyme sialyltransferase, and thus, the insect viruses produced are missing the terminal sialylation found in the vertebrate-grown virus (1, 46). This difference could result in the altered, more extended configuration of the BHK surface glycoproteins. The multishell model-fitting results for the innermost two layers also indicate a difference in the distributions of material within the core and inner capsid. The core of the C7-10 virus has a more compact RNA structure than that of the BHK virus, inferred from the higher scattering-length density (more D_2O) of the second shell. The results suggest that more RNA exists in the second shell in the BHK virus than in the C7-10 virus, suggesting that the RNA in the BHK virion has a stronger interaction with the nucleocapsid protein than in the C7-10 virion. These data suggest that Sindbis virus can adopt more than one metastable infectious conformation during assembly.

Conclusions. Sindbis viruses grown from mammalian and insect cells are assumed to have functionally equivalent structures, while the assembly pathways differ in certain details during the infection process (1, 46). The current work is the first demonstration that host-specific differences in virion

structure do exist, which supports recent work demonstrating that the host influences the composition of Sindbis virus (11).

The structures of the alphaviruses have been determined at moderate resolution using the technique of cryoEM and three-dimensional reconstruction (24, 32, 35–38, 43). These studies have been conducted on virus produced from mammalian cells. The dimensions of the components of the mammalian virus determined in these studies agree nicely with those reported here using the technique of small-angle neutron scattering. Because of the biological and immunological equivalence of viruses produced from the insect and mammalian cell types (31), we were surprised to find a significant difference in the structures of the insect-grown virions, particularly in the glycoprotein shell. The data seem to suggest that while functionally equivalent, the glycoproteins of the insect and mammalian-cell-grown virions exhibit subtle differences in configuration. The absence of cholesterol in the insect cell membrane (11) and the absence of terminal sialylation of the insect-produced carbohydrate side chains (47) may both contribute to the observed difference. This observation is particularly significant, as a crystal structure of the E1 glycoprotein truncated to remove the hydrophobic transmembrane domain has been fitted into the electron density map of the surface reconstruction of alphavirus produced from mammalian cells (32, 62). We have previously shown that the Sindbis virus E1 glycoprotein can exist in several disulfide-bridged configurations detected on nonreducing polyacrylamide gels after extraction of the protein from the intact virion (33). We have also shown that the structure of the E1 protein on the surface of the virion is not the same as that in the crystal structure (58). If the isolated E1 glycoprotein can assume a number of configurations, it is unclear which is capable of crystallization and which form exists in the surface of the mammal- or insect-produced virus. The possibility of species-dependent structural polymorphism of E1 in the intact virion is supported by the current work.

The modeling performed has made it possible to determine that not only does the Sindbis virus grown in BHK cells have cholesterol incorporated into the lipid layer, but the distribution of genetic material in the core of the virus depends on the host species. This observation is particularly intriguing and very difficult to explain. The core of the virion is composed of 240 copies of the capsid protein and the virus RNA. The RNA combines with the capsid protein to assemble preformed nucleocapsid structures that are then enveloped in the cellular membrane containing the virus glycoprotein (9). There are no known requirements for host cell components in the formation of the nucleocapsid, and assembly has been demonstrated *in vitro* (54, 56). The current result implies that the chemical environment provided by the host cell affects the assembly process. These results provide new insight into the natural cycle of Sindbis virus as it transitions between mammalian and insect hosts and suggest that the structural changes are important for the transition from one host to another.

This study also demonstrated the utility of SANS for probing structural differences between virus particles. In addition to providing sufficient sensitivity for detecting changes in structure, the lack of radiation damage ensures that the results are not influenced by loss of the structural integrity of the particle, as demonstrated by the unchanged infectivity after the SANS measurements. The ability to work in dilute solution also ensures that the results are free of artifacts that may be induced by the use of heavy metal stains, adsorption to a grid, or structural transitions driven during the process of crystallization. The methodology presented here is broadly applicable to other problems in structural virology and can provide new and unique insight into host-specific structural differences in other viruses that may be critical to their transition between biologically unrelated hosts.

ACKNOWLEDGMENTS

This research was sponsored by the Laboratory Directed Research and Development Program of Oak Ridge National Laboratory (ORNL) (F.M.). D.T.B. and R.H. are supported by The Foundation for Research, Carson City, NV. The research at ORNL's Center for Structural Molecular Biology (CSMB) was supported by the Office of Biological and Environmental Research, using facilities supported by the U.S. Department of Energy and managed by UT-Battelle, LLC, under contract no. DE-AC05-00OR22725.

REFERENCES

1. **Brown, D. T., and L. D. Condreay.** 1986. Replication of alphaviruses in mosquito cells, p. 171–207. *In* M. J. Schlesinger (ed.), The Togaveriridae and Flaviviridae. Plenum Publishing Corporation, New York, NY.
2. **Burge, B. W., and J. H. Strauss, Jr.** 1970. Glycopeptides of the membrane glycoprotein of Sindbis virus. J. Mol. Biol. **47:**449–466.
3. **Chauvin, C., B. Jacrot, and J. Witz.** 1977. Structure and molecular-weight of satellite tobacco necrosis virus: neutron small-angle scattering study. Virology **83:**479–481.
4. **Chauvin, C., J. Witz, and B. Jacrot.** 1978. Structure of Tomato Bushy Stunt Virus; model for protein-RNA interaction. J. Mol. Biol. **124:**641–651.
5. **Cuillel, M., C. Berthetcolominas, B. Krop, A. Tardieu, P. Vachette, and B. Jacrot.** 1983. Self-assembly of brome mosaic-virus capsids: kinetic-study using neutron and X-ray solution scattering. J. Mol. Biol. **164:**645–650.
6. **Cusack, S.** 1983. Neutron-scattering studies of virus structure. Institute of Physics Conference Series **64:**351–355.
7. **Cusack, S., A. Miller, P. C. J. Krijgsman, and J. E. Mellema.** 1981. An investigation of the structure of alfalfa mosaic-virus by small-angle neutron-scattering. J. Mol. Biol. **145:**525–543.
8. **Cusack, S., R. W. H. Ruigrok, P. C. J. Krygsman, and J. E. Mellema.** 1985. Structure and composition of influenza-virus: a small-angle neutron-scattering study. J. Mol. Biol. **186:**565–582.
9. **Ferreira, D. F., R. Hernandez, M. Horton, and D. T. Brown.** 2003. Morphological variants of Sindbis virus produced by a mutation in the capsid protein. Virology **307:**54–66.
10. **Guinier, A., and G. Fournet (ed.).** 1955. Small angle scattering of X-rays. Willey, New York, NY.
11. **Hafer, A., R. Whittlesey, D. T. Brown, and R. Hernandez.** 2009. Differential incorporation of cholesterol by Sindbis virus grown in mammalian or insect cells. J. Virol. **83:**9113–9121.
12. **Harrison, S. C., A. David, J. Jumblatt, and J. E. Darnell.** 1971. Lipid and protein organization in Sindbis virus. J. Mol. Biol. **60:**523–524.
13. **Hernandez, R., H. Lee, C. Nelson, and D. T. Brown.** 2000. A single deletion in the membrane-proximal region of the Sindbis virus glycoprotein E2 endodomain blocks virus assembly. J. Virol. **74:**4220–4228.
14. **Hernandez, R., C. Sinodis, and D. T. Brown.** 2005. Sindbis virus: propagation, quantification, and storage. Curr. Protoc Microbiol. Chapter **15:**Unit 15B 1.
15. **Hernandez, R., C. Sinodis, M. Horton, D. Ferreira, C. Yang, and D. T. Brown.** 2003. Deletions in the transmembrane domain of a Sindbis virus glycoprotein alter virus infectivity, stability, and host range. J. Virol. **77:** 12710–12719.
16. **Inoue, H., and P. A. Timmins.** 1985. The structure of rice dwarf virus determined by small-angle neutron-scattering measurements. Virology **147:** 214–216.
17. **Jacrot, B.** 1976. Study of biological structures by neutron-scattering from solution. Rep. Prog. Phys. **39:**911–953.
18. **Jacrot, B., C. Chauvin, and J. Witz.** 1977. Comparative neutron small-angle scattering study of small spherical RNA viruses. Nature **266:**417–421.
19. **Kline, S. R.** 2006. Reduction and analysis of SANS and USANS data using IGOR Pro. J. Appl. Crystallogr. **39:**895–900.
20. **Knight, R. L., K. L. Schultz, R. J. Kent, M. Venkatesan, and D. E. Griffin.** 2009. Role of N-linked glycosylation for Sindbis virus infection and replication in vertebrate and invertebrate systems. J. Virol. **83:**5640–5647.
21. **Kruse, J., P. A. Timmins, and J. Witz.** 1982. A neutron-scattering study of the structure of compact and swollen forms of southern bean mosaic-virus. Virology **119:**42–50.

22. **Kuzmanovic, D. A., I. Elashvili, C. Wick, C. O'Connell, and S. Krueger.** 2003. Bacteriophage MS2: molecular weight and spatial distribution of the protein and RNA components by small-angle neutron scattering and virus counting. Structure **11:**1339–1348.
23. **Leimkuhler, M., A. Goldbeck, M. D. Lechner, and J. Witz.** 2000. Conformational changes preceding decapsidation of bromegrass mosaic virus under hydrostatic pressure: a small-angle neutron scattering study. J. Mol. Biol. **296:**1295–1305.
24. **Lescar, J., A. Roussel, M. W. Wien, J. Navaza, S. D. Fuller, G. Wengler, and F. A. Rey.** 2001. The fusion glycoprotein shell of Semliki Forest virus: an icosahedral assembly primed for fusogenic activation at endosomal pH. Cell **105:**137–148.
25. **Liu, L. N., H. Lee, R. Hernandez, and D. T. Brown.** 1996. Mutations in the endo domain of Sindbis virus glycoprotein E2 block phosphorylation, reorientation of the endo domain, and nucleocapsid binding. Virology **222:**236–246.
26. **Liu, N., and D. T. Brown.** 1993. Transient translocation of the cytoplasmic (endo) domain of a type I membrane glycoprotein into cellular membranes. J. Cell Biol. **120:**877–883.
27. **Lopez, S., J. S. Yao, R. J. Kuhn, E. G. Strauss, and J. H. Strauss.** 1994. Nucleocapsid-glycoprotein interactions required for assembly of alphaviruses. J. Virol. **68:**1316–1323.
28. **Lu, Y. E., T. Cassese, and M. Kielian.** 1999. The cholesterol requirement for Sindbis virus entry and exit and characterization of a spike protein region involved in cholesterol dependence. J. Virol. **73:**4272–4278.
29. **Lynn, G. W., W. Heller, V. Urban, G. D. Wignall, K. Weiss, and D. A. A. Myles.** 2006. Bio-SANS: a dedicated facility for neutron structural biology at Oak Ridge National Laboratory. Physica B **86:**880–882.
30. **Marquardt, M. T., T. Phalen, and M. Kielian.** 1993. Cholesterol is required in the exit pathway of Semliki Forest virus. J. Cell Biol. **123:**57–65.
31. **Moore, N. F., Y. Barenholz, and R. R. Wagner.** 1976. Microviscosity of togavirus membranes studied by fluorescence depolarization: influence of envelope proteins and the host cell. J. Virol. **19:**126–135.
32. **Mukhopadhyay, S., W. Zhang, S. Gabler, P. R. Chipman, E. G. Strauss, J. H. Strauss, T. S. Baker, R. J. Kuhn, and M. G. Rossmann.** 2006. Mapping the structure and function of the E1 and E2 glycoproteins in alphaviruses. Structure **14:**63–73.
33. **Mulvey, M., and D. T. Brown.** 1994. Formation and rearrangement of disulfide bonds during maturation of the Sindbis virus E1 glycoprotein. J. Virol. **68:**805–812.
34. **Nagle, J. F., and S. Tristram-Nagle.** 2000. Structure of lipid bilayers. Biochim. Biophys. Acta **1469:**159–195.
35. **Paredes, A., K. Alwell-Warda, S. C. Weaver, W. Chiu, and S. J. Watowich.** 2001. Venezuelan equine encephalomyelitis virus structure and its divergence from Old World alphaviruses. J. Virol. **75:**9532–9537.
36. **Paredes, A. M., D. T. Brown, R. Rothnagel, W. Chiu, R. J. Schoepp, R. E. Johnston, and B. V. Prasad.** 1993. Three-dimensional structure of a membrane-containing virus. Proc. Natl. Acad. Sci. U. S. A. **90:**9095–9099.
37. **Paredes, A. M., D. Ferreira, M. Horton, A. Saad, H. Tsuruta, R. Johnston, W. Klimstra, K. Ryman, R. Hernandez, W. Chiu, and D. T. Brown.** 2004. Conformational changes in Sindbis virions resulting from exposure to low pH and interactions with cells suggest that cell penetration may occur at the cell surface in the absence of membrane fusion. Virology **324:**373–386.
38. **Paredes, A. M., H. Heidner, P. Thuman-Commike, B. V. Prasad, R. E. Johnston, and W. Chiu.** 1998. Structural localization of the E3 glycoprotein in attenuated Sindbis virus mutants. J. Virol. **72:**1534–1541.
39. **Phalen, T., and M. Kielian.** 1991. Cholesterol is required for infection by Semliki Forest virus. J. Cell Biol. **112:**615–623.
40. **Putnam, C. D., M. Hammel, G. L. Hura, and J. A. Tainer.** 2007. X-ray solution scattering (SAXS) combined with crystallography and computation: defining accurate macromolecular structures, conformations and assemblies in solution. Q. Rev. Biophys. **40:**191–285.
41. **Renkonen, O., C. G. Gahmberg, K. Simons, and L. Kaariainen.** 1972. The lipids of the plasma membranes and endoplasmic reticulum from cultured baby hamster kidney cells (BHK21). Biochim. Biophys. Acta **255:**66–78.
42. **Renkonen, O., L. Kaarainen, K. Simons, and C. G. Gahmberg.** 1971. The lipid class composition of Semliki Forest virus and plasma membranes of the host cells. Virology **46:**318–326.
43. **Roussel, A., J. Lescar, M. C. Vaney, G. Wengler, G. Wengler, and F. A. Rey.** 2006. Structure and interactions at the viral surface of the envelope protein E1 of Semliki Forest virus. Structure **14:**75–86.
44. **Sato, M., Y. Ito, K. Kameyama, M. Imai, N. Ishikawa, and T. Takagi.** 1995. Small-angle neutron-scattering study of recombinant yeast-derived human hepatitis-B virus surface-antigen vaccine particle. Physica B **213:**757–759.
45. **Semenyuk, A. V., and D. I. Svergun.** 1991. Gnom: a program package for small-angle scattering data processing. J. Appl. Crystallogr. **24:**537–540.
46. **Stollar, V. (ed.).** 1980. Togaviruses in cultured arthropod cells. Acedemic Press, Inc., New York, NY.
47. **Stollar, V., B. D. Stollar, R. Koo, K. A. Harrap, and R. W. Schlesinger.** 1976. Sialic acid contents of Sindbis virus from vertebrate and mosquito cells. Virology **69:**104–115.
48. **Strauss, J. H., and E. G. Strauss.** 1994. The alphaviruses: gene expression, replication, and evolution. Microbiol. Rev. **58:**491–562.
49. **Stubbs, M. J., A. Miller, P. J. H. Sizer, J. R. Stephenson, and A. J. Crooks.** 1991. X-ray solution scattering of Sindbis virus: changes in conformation induced at low pH. J. Mol. Biol. **221:**39–42.
50. **Stuhrman, H.** 1974. Neutron small-angle scattering of biological macromolecules in solution. J. Appl. Crystallogr. **7:**173–178.
51. **Svergun, D. I.** 2007. Small-angle scattering studies of macromolecular solutions. J. Appl. Crystallogr. **40:**S10–S17.
52. **Svergun, D. I., and M. H. J. Koch.** 2002. Advances in structure analysis using small-angle scattering in solution. Curr. Opin. Struct. Biol. **12:**654–660.
53. **Svergun, D. I., and M. H. J. Koch.** 2003. Small-angle scattering studies of biological macromolecules in solution. Rep. Prog. Phys. **66:**1735–1782.
54. **Tellinghuisen, T. L., R. Perera, and R. J. Kuhn.** 2001. In vitro assembly of Sindbis virus core-like particles from cross-linked dimers of truncated and mutant capsid proteins. J. Virol. **75:**2810–2817.
55. **Timmins, P. A., and G. Zaccai.** 1988. Low resolution structures of biological complexes studied by neutron-scattering. Eur. Biophys. J. Biophy. **15:**257–268.
56. **Wengler, G., U. Boege, H. Bischoff, and K. Wahn.** 1982. The core protein of the alphavirus Sindbis virus assembles into core-like nucleoproteins with the viral genome RNA and with other single-stranded nucleic acids in vitro. Virology **118:**401–410.
57. **West, J., R. Hernandez, D. Ferreira, and D. T. Brown.** 2006. Mutations in the endodomain of Sindbis virus glycoprotein E2 define sequences critical for virus assembly. J. Virol. **80:**4458–4468.
58. **Whitehurst, C. B., E. J. Soderblom, M. L. West, R. Hernandez, M. B. Goshe, and D. T. Brown.** 2007. Location and role of free cysteinyl residues in the Sindbis virus e1 and e2 glycoproteins. J. Virol. **81:**6231–6240.
59. **Whitehurst, C. B., J. H. Willis, C. N. Sinodis, R. Hernandez, and D. T. Brown.** 2006. Single and multiple deletions in the transmembrane domain of the Sindbis virus E2 glycoprotein identify a region critical for normal virus growth. Virology **347:**199–207.
60. **Wignall, G. D., and F. S. Bates.** 1987. Absolute calibration of small-angle neutron-scattering data. J. Appl. Crystallogr. **20:**28–40.
61. **Zaccai, G.** 1986. Measurement of density and location of solvent associated with biomolecules by small-angle neutron-scattering. Methods Enzymol. **127:**619–629.
62. **Zhang, W., S. Mukhopadhyay, S. V. Pletnev, T. S. Baker, R. J. Kuhn, and M. G. Rossmann.** 2002. Placement of the structural proteins in Sindbis virus. J. Virol. **76:**11645–11658.